https://doi.org/10.1007/s41230-022-9003-2

An Al-12Si/ZnS powder inoculant for eutectic silicon in Al-12Si alloy

Ying Wang, Pan-yu Chen, Yu-hui Lin, and *Cheng-dong Li

College of Materials Science and Engineering, Qingdao University of Science &Technology, Qingdao 266042, China

Abstract: To obtain high-performance Al-Si-based cast alloys, refinement and modification of Si phases are required. An Al-12Si/ZnS powder inoculant was designed and fabricated using a chemical bath deposition method. The efficiency of the inoculant for modifying the eutectic Si phase in as-cast Al-12Si alloy was studied. Results show that Al-12Si/ZnS powder can significantly refine the eutectic Si in Al-Si cast alloys. The best refinement effect for eutectic Si was achieved with 17.5% Al-12Si/ZnS powder. Coarse long needle-shaped eutectic Si with a length of 18 μm was modified into approximately spherical shape with a diameter of 7 μm, which was evenly distributed throughout the alloy. The E2EM model calculation indicates that the inter-plane misfit (F_p) and inter-atomic spacing misfit (F_r) between ZnS and Si are all less than 0.5%, which confirms that ZnS is a potential nucleation site for Si phases. The hardness, tensile strength, and elongation of Al-12Si alloys modified with 17.5% Al-12Si/ZnS powder increase 6.3%, 16.19% and 55.35%, respectively, compared to the unmodified Al-12Si alloy. The fracture behavior of the alloy with 17.5% Al-12Si/ZnS powder was dominated by transgranular fracture supplemented by intergranular fracture.

Keywords: Al-Si; Al-Si/ZnS; refinement; eutectic silicon

CLC numbers: TG146.21 **Document code:** A **Article ID:** 1672-6421(2021)01-081-10

1 Introduction

In recent decades, aluminum-silicon (Al-Si)-based cast alloys have been extensively used in the automobile industry owing to their many advantages, such as low coefficient of thermal expansion, good wear resistance, and light weight, which can help meet energy conservation and emissions reduction requirements [1-3]. The high Si content improves the fluidity of eutectic Al-Si alloys, resulting in good casting properties [4]. However, a large amount of long, coarse needle-like eutectic Si in the microstructure can seriously dissever the matrix and adversely affect the mechanical properties of the alloy [5, 6]. Therefore, it is necessary to refine and modify eutectic Si to improve the mechanical and machining properties of hypereutectic and eutectic Al-Si-based cast alloys. There are two principal mechanisms for modification of eutectic Si: growth theory and nucleation theory [7]. Based on these theories, many strategies have been investigated for achieving grain refinement or modifying the long, coarse needle-shaped Si in Al-Si alloys [8]. Techniques such as melt quenching via rapid cooling, semi-solid state processing, melt shearing technologies based on ultrasonic vibrations or external fields, and chemical modification via the addition of certain elements have been proven to be efficient methods for refining the eutectic Si structure in Al-Si alloys [9-16]. In particular, adding chemical modifiers to refine the alloy is a simple and efficient method for industrial production [17, 18]. To date, investigators have mainly focused on eutectic Si modification by chemical modifiers [19]. The morphology of eutectic Si can be modified by adding chemical modifiers such as Na, La, Sb and Sr to the melt, which inhibit the growth of eutectic silicon, to achieve refinement [20-24]. Liu et al. [25] reported that adding Sr to the A356 melt decreased the eutectic temperature, increased the volume fraction of the α-Al phase, and shortened the dendrite lengths. However, the industrial application of chemical modifiers remains limited due to potential side effects, such as more oxide inclusions by adding Sr into the Al-Si alloy. So, it is necessary to develop a new simple, efficient, and low-cost heterogeneous nucleating agent for refining eutectic Si in Al-Si alloys.

Zinc sulfide (ZnS) is a relatively new inoculant being used to refine Si in Al-Si alloys. Kawther et al. [26-28] reported the refinement of ZnS on primary Si in

***Cheng-dong Li**

Male, born in 1973, Ph.D. Research interests: melting, casting and powder metallurgy preparation, grain refinement and particle reinforcement of high performance aluminum alloys.

E-mail: lichengdong@qust.edu.cn

Received: 2021-01-03; Accepted: 2021-09-27

hypereutectic Al-Si alloy. The Al-ZnS master alloy was prepared by in situ reaction of Zn and Na_2S in the Al melt, and then was used to refine the primary Si in Al-22Si alloy [26]. The mechanism of primary Si refinement using ZnS particles and Al-ZnS master alloy in Al-24Si cast alloy was studied [27, 28]. The degree of lattice mismatch between Si (5.421 Å) and ZnS, which exists as a face centered cubic lattice structure with a lattice constant of 5.410 Å below 1,020 °C, is 0.20% [29]. Hence, according to heterogeneous nucleation theory, ZnS is a promising nucleus for the Si phase, and can simultaneously refine primary and eutectic Si. What is more, in our previous experiments, a phenomenon was found that the morphology of some eutectic Si changed from long needle-like to short rod-like by adding micro-nano ZnS particles into the Al-24Si alloy. So, developing a ZnS modifier for refining eutectic Si becomes possible. However, there are few reports on eutectic Si refinement using ZnS. Quested et al. [30] recently verified a model which could predict the grain size in Al alloys with commercial refiner. They found grain size of Al alloy decreased at first and then increased when the size of the refiner (TiB_2) particles increased in the range of 0–6 μm. Similarly, the modification effect of ZnS on eutectic Si should also be related to the particle size of ZnS, and the refinement of eutectic Si could be achieved only when the particle size of ZnS is at the nanometer level. In addition, it is reported that the particle size of nano-sized ZnS particles prepared by chemical water bath deposition methods was easily controlled by adjusting reaction time [31, 32]. Therefore, design and synthesis of nano-sized ZnS on the matrix using the chemical water bath deposition method is feasible.

This study aims to design and synthesize an inoculant Al-12Si/ZnS to provide nuclei for eutectic silicon. The Al-12Si/ZnS powder was prepared via a simple chemical water bath deposition method using tri-sodium citrate and tartaric acid as complexing agents. The size and morphology of eutectic Si in the Al-12Si alloy were modified by the addition of Al-12Si/ZnS powder. The effect of different Al-12Si/ZnS additions on the refinement of eutectic Si in Al-12Si alloy is compared, the morphology of eutectic silicon is observed, the grain size and area of eutectic silicon are analyzed. Tensile testing and analysis of alloy fracture mechanism are performed.

2 Experimental

2.1 Materials

Commercial pure Al alloy (99.5wt.% purity), Al-24Si alloy (99.95wt.% purity) and Al-12Si powder (99.995wt.% purity, 90% of the particles are 34–70 μm in size) were used. The chemical composition of the Al-24Si alloy, pure Al and Al-24Si powder are given in Table 1.

Table 1: Chemical compositions of Al-12Si, Al-24Si alloys and Al-12Si powder (wt.%)

Alloy	Si	Mg	Mn	Cu	Fe	Ti	Al
Al-24Si	24	0.0373	0.043	0.003	0.197	0.0167	Bal.
Pure Al	0.003	-	-	0.003	0.005	-	Bal.
Al-12Si powder	12	-	-	-	0.15	-	Bal.

2.2 Preparation of Al-12Si/ZnS inoculant

Figure 1 shows a schematic illustration of the Al-12Si/ZnS preparation process. First, 0.728 g of ZnS was completely dissolved in 20 mL distilled water, 0.249 g thiocarbamide was dissolved in 10 mL distilled water, 0.24 g tartaric acid was dissolved in 10 mL distilled water, and 0.249 g trisodium citrate was dissolved in 10 mL distilled water. Next, the zinc sulfate solution, tartaric acid solution, and trisodium citrate solution were mixed in a 100 mL beaker by magnetic stirring. Subsequently, the thiocarbamide solution was slowly dripped into the mixture, then 15 g Al-12Si alloy powder was added. The pH value was adjusted to about 10 with ammonium hydroxide, and the solution was placed in a water bath at 80 °C and stirred for 0.5 h. Finally, the solution was filtered, washed, and vacuum dried at 50 °C to obtain the Al-12Si/ZnS powder.

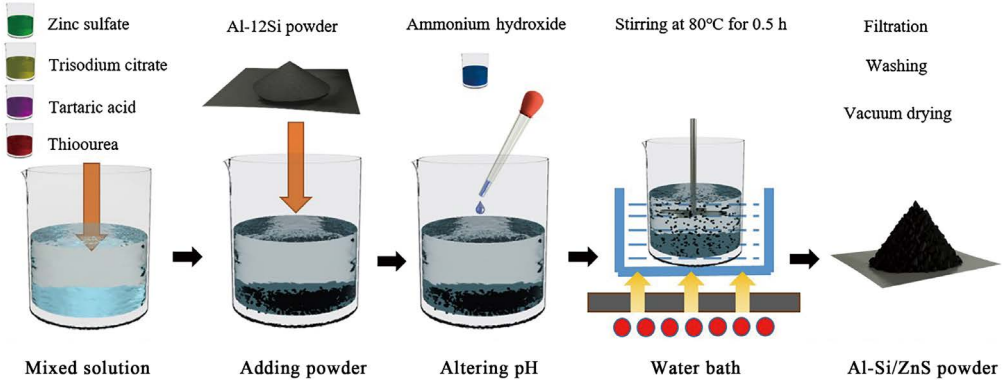

Fig. 1: Schematic illustration of preparation of Al-12Si/ZnS inoculant preparation

2.3 Melt processing

Figure 2 shows the preparation of Al-12Si alloy modified with Al-12Si/ZnS powder. The Al-12 Si alloy in a graphite crucible was firstly heated to 900 °C, and held for 15 min. Then, the alloy was modified by adding different amounts of Al-12Si/ZnS powder (12.5wt.%, 17.5wt.%, 22.5wt.%) at 730 °C, manually stirred for 30 s, then held for an additional 10 min. Finally, the molten metal was skimmed and poured into a metal die (preheated at 200 °C for 2 h). According to the GB/T228.1-2010, the tensile testing was carried out using the rod-shaped specimens with a diameter of 10 mm, as shown in Fig. 3.

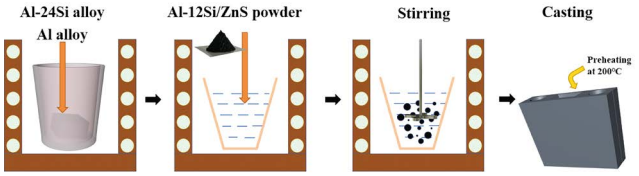

Fig. 2: Preparation of Al-12Si alloy modified with Al-12Si/ZnS powder

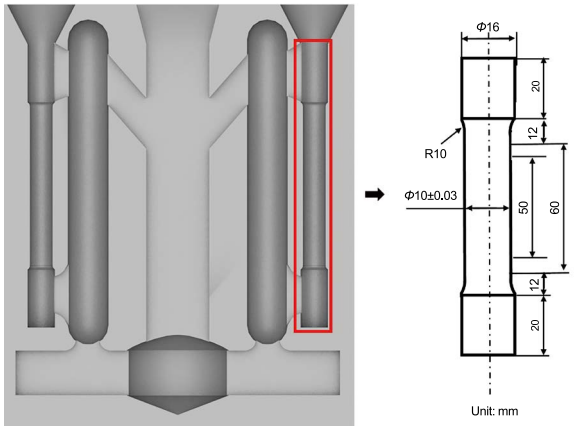

Fig. 3: Shape and size of tensile test specimen

The crystal structure of the synthesized Al-12Si/ZnS powder was characterized using a Rigaku D/Max-2200 X-ray diffractometer with Cu Kα radiation (λ=1.5406Å) at room temperature within the range 2θ of 10–80°. The powder morphology was observed using scanning electron microscopy (SEM, JSM-6700F, JEOL, Japan), and the elemental content of the powder were determined by energy dispersive X-ray spectroscopy (EDX). The transmission electron microscopy (TEM, JEM-2100, JEOL) and high-resolution transmission electron microscopy (HRTEM) were employed to observe the morphology of ZnS growing on the surface of the Al-12Si/ZnS powder. The microstructure of Al-12Si alloy was observed and characterized using SEM and optical microscopy (OM; XJP-200, Jiangnan) and analyzed with software provided by Nanjing Jiangnan Novel Optics Co., Ltd. The HB hardness of the Al-12Si alloy was measured using a Brinell hardness tester (320HBS-3000, Laizhou Hayin Testing Instrument Co., Ltd., China) at a load of 1,000 g for 30 s, and the tensile testing of the Al-12Si alloy was performed on a Taiwan SARTEC SS-8900 testing machine.

3 Results and discussion

3.1 Phase analysis and morphology of Al-12Si/ZnS powder

The XRD patterns are shown in Fig. 4. As shown in Fig. 4(a), there is only one diffraction peak in the X-ray diffraction spectrum of the monocrystalline Si slice/ZnS at 2θ=69.10°, which is identical to the (400) planes of cubic Si (PDF#27–1402) and ZnS (PDF#05–0506). It is difficult to distinguish the ZnS peak since the peak positions are almost exactly the same. In Fig. 4(b), three main diffraction peaks can be observed at 2θ=28.62°, 47.80°, and 56.36°, which are identical to the (111), (220), and (311) planes of cubic Si (PDF#27–1402) and ZnS (PDF#05–0506), respectively. In Fig. 4(c), the XRD pattern of the Al-12Si/ZnS powder has strong diffraction peaks at 2θ=38.46°, 44.72°, 65.10°, and 78.26°, which are identical to cubic Al (PDF#04–0787), and at 2θ=28.42°, 47.30°, and 56.16°, which are identical to cubic Si and ZnS. Certainly, amorphous peaks as marked by the arrows can be observed in all samples. According to the XRD results, it can be concluded that ZnS has the same crystal orientation with the Si phase.

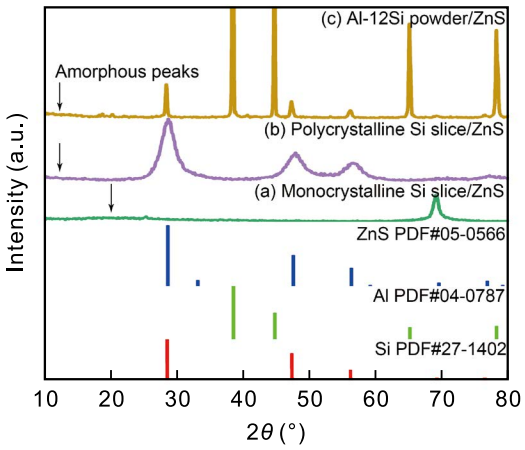

Fig. 4: X-ray diffraction spectra of as-prepared monocrystalline Si slice/ZnS (a), polycrystalline Si slice/ZnS (b), Al-12Si/ZnS powder (c)

To find evidence of the presence of ZnS, the Al-12Si/ZnS powder was also analyzed by EDX, as shown in Fig. 5. A uniform distribution of Al, Si, Zn, and S elements can be confirmed. Locations where there is more Si element also correspond to more S and Zn elements. In other words, the Si phase distribution affects the ZnS distribution. The combination of XRD patterns and EDX mapping images reveals that the powder is composed of Al-12Si and ZnS. It can be inferred that ZnS particles successfully deposited on the surface of Al-Si powder and can act as the nucleus of Si due to the similar crystal structure of ZnS and Si.

As shown in Fig. 6(a), the Al-12Si/ZnS powder is composed of Al-Si spheres with diameters of about 70–80 μm. As shown in the enlarged image in Fig. 6(b), a large number of ZnS particles form on the surface of the Al-Si spheres. The image was further magnified and Figs. 6(c) and (d) show the enlarged circular and rectangular regions in Fig. 6(b), respectively. Both

of the magnified images show a large number of ZnS particles with diameters of about 10–40 nm formed by Volmer-Weber (VW) growth and evenly distributed on the surface of the Al-12Si/ZnS spheres [33]. The above analyses show that Al-12Si/ZnS was successfully prepared.

Further characterization of the microstructure and morphology of the Al-12Si/ZnS powder was performed using TEM and HRTEM. Figures 7(a)–(c) show the TEM images of the powder at a low magnification. Figure 7(a) shows a nearly spherical particle with a diameter of about 45 μm. In Figs. 7(b) and (c), a large number of particles can be observed on the surface of the powder. High-magnification TEM images are presented in Figs. 7(d)-(e). Some high contrast areas can be observed, marked by dotted circles and surrounded by areas of weak contrast, which are consistant with the SEM results. The degree of constancy is related to the level of crystallinity, therefore, in the amorphous ZnS region, the degree of constancy is weaker. Lattice fringes are clearly visible in the HRTEM images of the particles, as shown in Figs. 7(f) and (g). The lattice spacings are about 0.285, 0.128, and 0.218 nm which are consistent with the *d*-spacing of (111), (311), and (220) planes of cubic ZnS, respectively. Based on the XRD, SEM, and EDS results, the as-prepared powder consists of an Al-Si alloy matrix with a large number of ZnS nanoparticles on the surface.

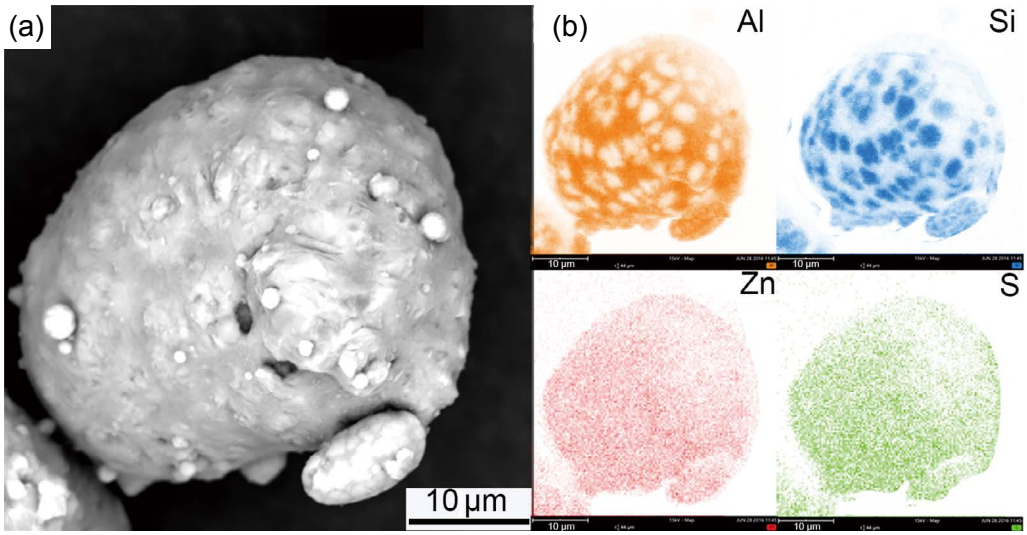

Fig. 5: SEM images of Al-12Si/ZnS power (a) and EDX elemental mapping images of Al, Si, Zn and S (b)

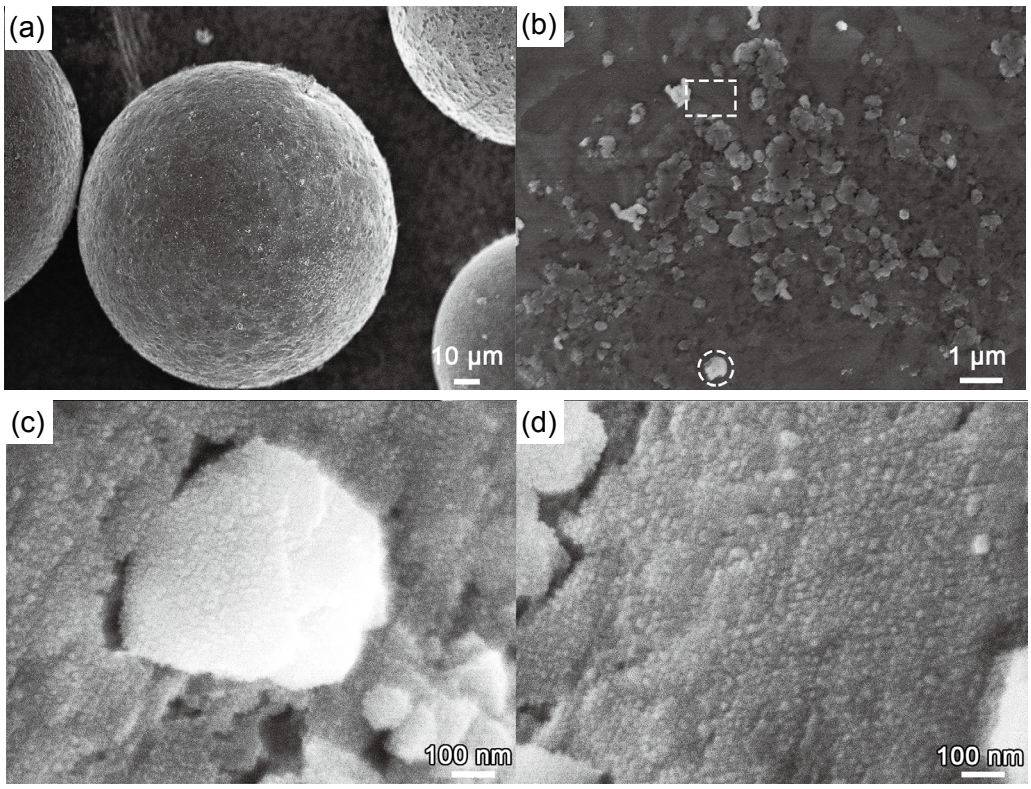

Fig. 6: SEM images of Al-12Si/ZnS powder, (c) and (d) are enlarged images of circular and rectangular regions in (b), respectively

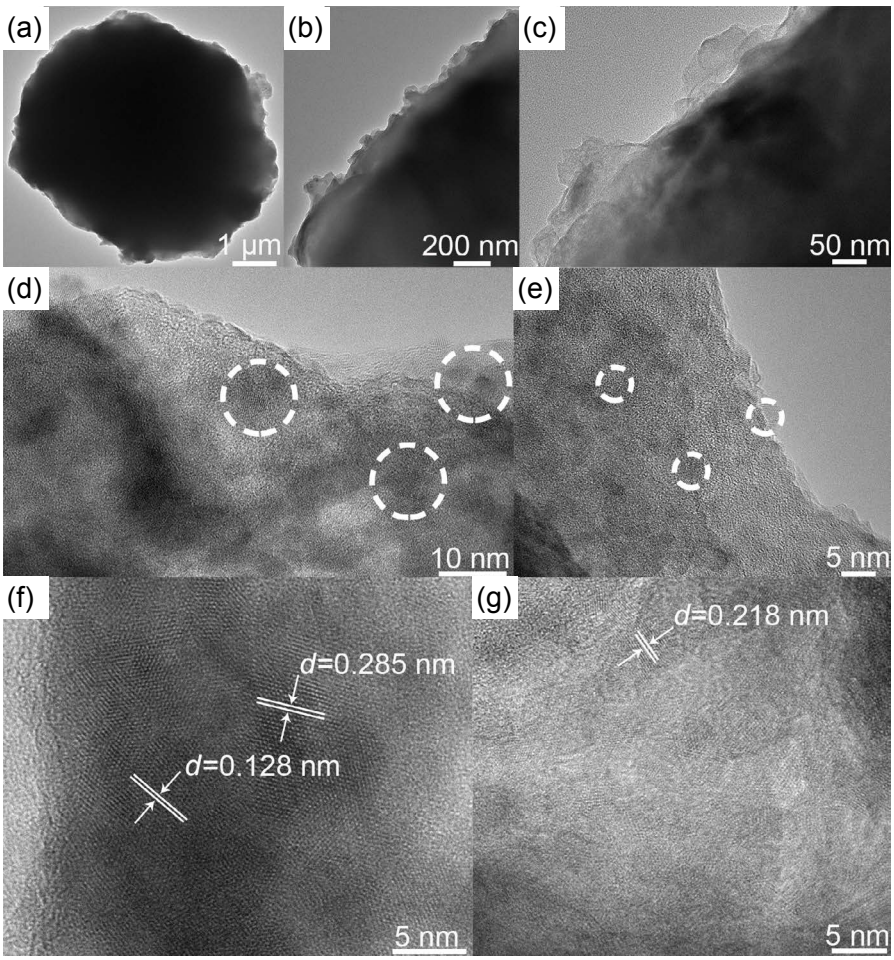

Fig. 7: Morphology and characterization of as-prepared Al-12Si/ZnS powder: TEM images (a–e), HRTEM images (f–g)

3.2 Effects of Al-12Si/ZnS powder addition amount on modification of eutectic silicon

Figure 8 shows the microstructures of Al-12Si alloys modified with different amounts of Al-12Si/ZnS powder (ranging from 0–22.5wt.%). Figure 9 shows the corresponding area and size distribution of eutectic Si. The typical needle-like morphology of eutectic Si is shown in Fig. 8(a). The corresponding mean area and average size are 76.64 μm^2 and 18.01 μm, respectively, as shown in Figs. 9(a) and (e). The eutectic Si is refined into short rods when 12.5wt.% Al-12Si/ZnS powder was added, as shown in Fig. 8(b), with a mean area and average size of 34.91 μm^2 and 12.19 μm, respectively, according to Figs. 9(b) and (f). In addition, the α-Al phase is also refined. As illustrated in Fig. 8(c), after adding 17.5wt.% Al-12Si/ZnS powder, the size of the α-Al and eutectic Si phases are further refined, and the morphology of eutectic Si obviously changes from rod-like to granular. The area and distribution size of the eutectic Si phases decrease to 13.53 μm^2 and 6.53 μm, respectively, as shown in Figs. 9(c) and (g). However, as more Al-12Si/ZnS is added, the eutectic Si is not further refined and its morphology degenerates from granular to short rod shape. As shown in Figs. 9(d) and (h), the mean area and average size of eutectic Si are 20.93 μm^2 and 10.17 μm, respectively. In general, the needle-like eutectic Si can be refined into small, short rod-like or spherical morphologies with an appropriate amount of Al-12Si/ZnS powder, which in the present study is about 17.5wt.%.

3.3 Hardness and mechanical properties of Al-12Si alloy modified with different amounts of Al-12Si/ZnS powder

3.3.1 Hardness and tensile properties

Figure 10(a) presents the HB hardness values of the unmodified and modified Al-12Si alloys. The modified Al-12Si alloys have higher hardness values than the non-modified alloy as a result of fine-grain strengthening. The maximum hardness is achieved with 17.5wt.% Al-12Si/ZnS, an increase of 6.3% compared with the unmodified specimen. Compared with the specimen modified with 17.5wt.% Al-12Si/ZnS, the hardness value of the specimens modified with 22.5wt.% Al-12Si/ZnS is lower due to grain coarsening.

The mechanical properties of Al-12Si alloys modified with different amounts of Al-12Si/ZnS powder are presented in Figs. 10(b) and (c). The tensile strength and elongation of the unmodified Al-12Si alloy are 118.45 MPa and 10.19%, respectively. The tensile strength and elongation increase when 12.5wt.% Al-12Si/ZnS powder is added. The alloy modified with 17.5wt.% Al-12Si/ZnS powder exhibits the highest tensile strength, 137.62 MPa, an increase of 16.19% compared to the unmodified Al-12Si alloy, and the elongation increases

55.35%. The alloy modified with 22.5wt.% Al-12Si/ZnS powder exhibits the largest elongation, and its tensile strength and elongation increase 11.81% and 58.72%, respectively, compared to the unmodified Al-12Si alloy.

Results mentioned above show that eutectic Si modification via the addition of Al-12Si/ZnS powder leads to a significant improvement in the mechanical properties of Al-12Si alloy, in particular, an increase in ductility.

3.3.2 Fracture characteristics

The tensile fracture morphologies of Al-12Si alloys modified with different amounts of Al-12Si/ZnS powder (0, 12.5, 17.5, and 22.5 wt.%) are presented in Fig. 11. Vast cleavage planes

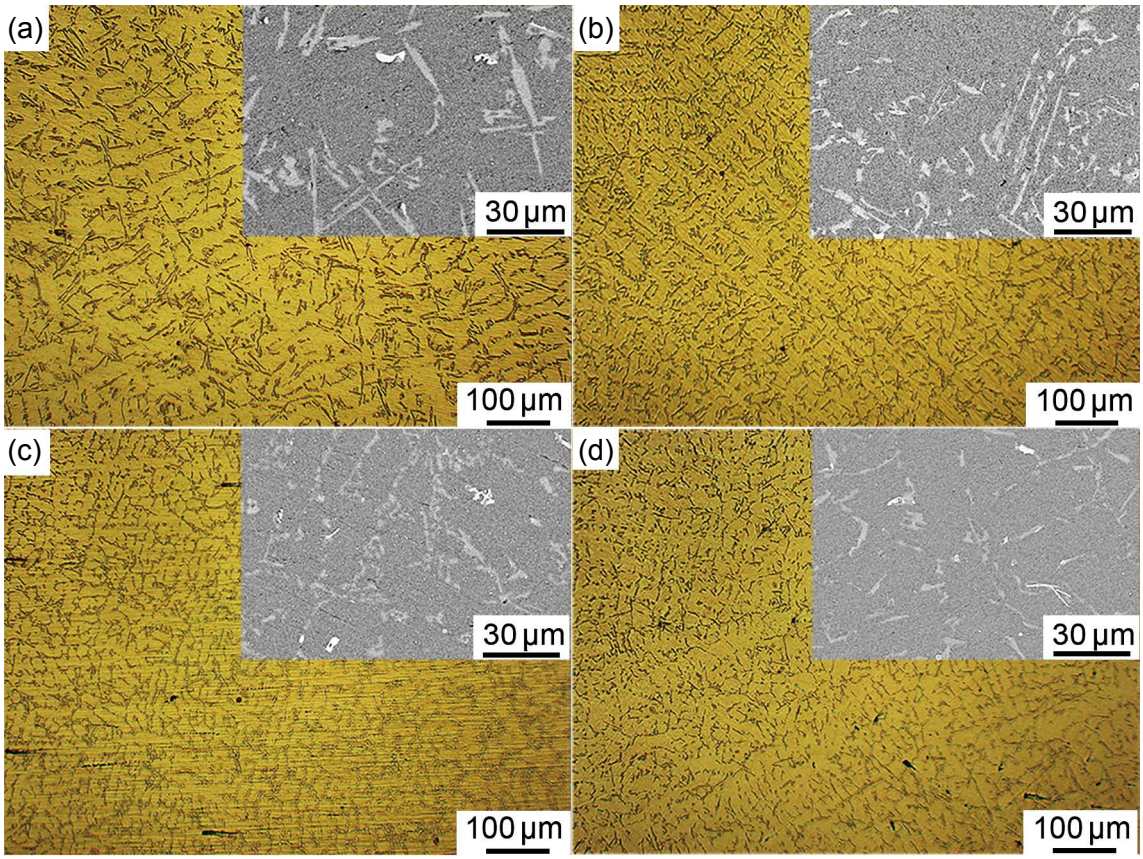

Fig. 8: Microstructures of Al-12Si alloys modified by different amounts of Al-12Si/ZnS powder: (a) unmodified; (b) 12.5wt.%; (c) 17.5wt.%; (d) 22.5wt.%

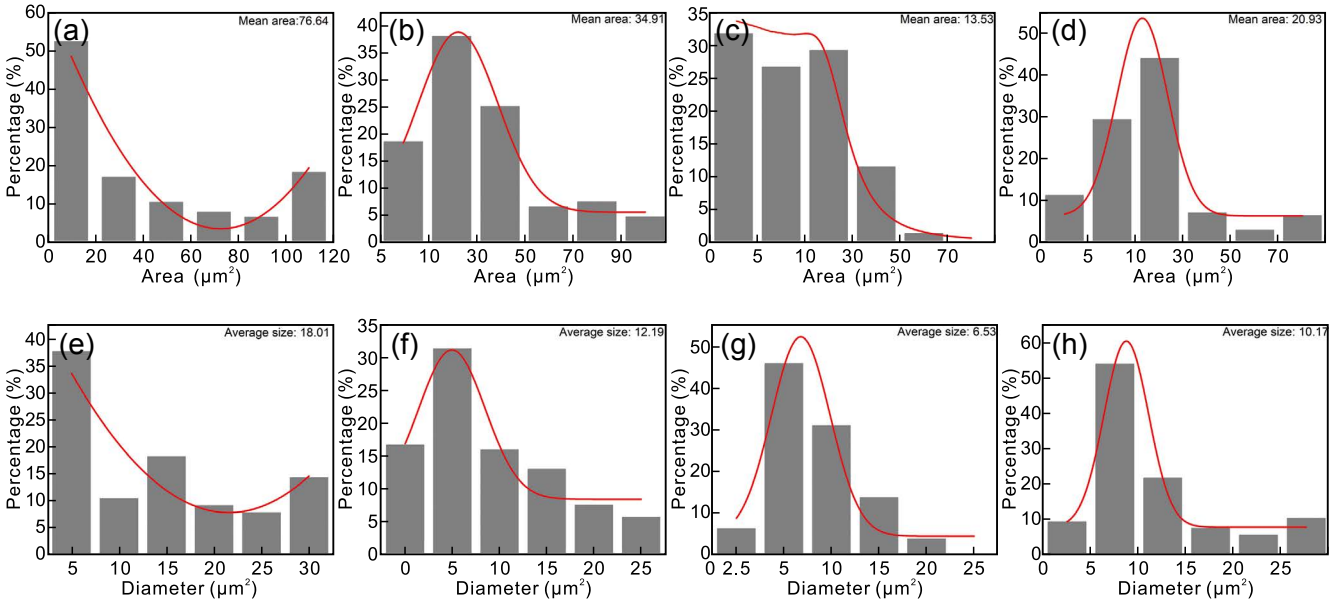

Fig. 9: Particle area distribution (a)-(d) and size distribution of eutectic silicon (e)-(h) in Al-12Si alloys modified by different amounts of Al-12Si/ZnS powder: (a) and (e) non-modified; (b) and (f) 12.5 wt.%; (c) and (g) 17.5 wt.%; (d) and (h) 22.5 wt.%

55.35%. The alloy modified with 22.5wt.% Al-12Si/ZnS powder exhibits the largest elongation, and its tensile strength and elongation increase 11.81% and 58.72%, respectively, compared to the unmodified Al-12Si alloy.

Results mentioned above show that eutectic Si modification via the addition of Al-12Si/ZnS powder leads to a significant improvement in the mechanical properties of Al-12Si alloy, in particular, an increase in ductility.

3.3.2 Fracture characteristics

The tensile fracture morphologies of Al-12Si alloys modified with different amounts of Al-12Si/ZnS powder (0, 12.5, 17.5, and 22.5 wt.%) are presented in Fig. 11. Vast cleavage planes on the surface indicate transgranular fracture of the unmodified alloy, as shown Fig. 11(a). Meanwhile, crystalline fracture

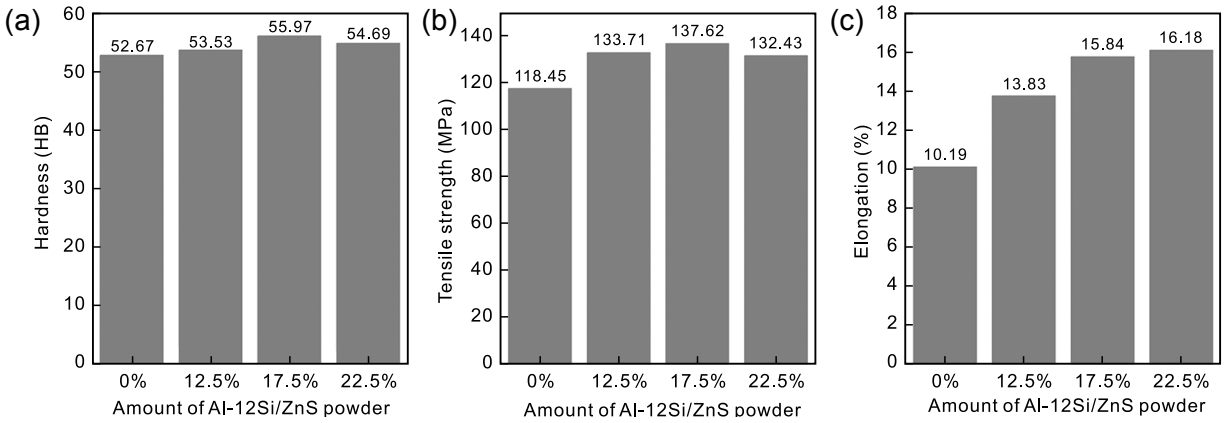

Fig. 10: Hardness and tensile properties of Al-12Si alloys modified with different amounts of Al-12Si/ZnS powder (0, 12.5, 17.5, and 22.5 wt. %): (a) HB hardness; (b) tensile strength; (c) elongation

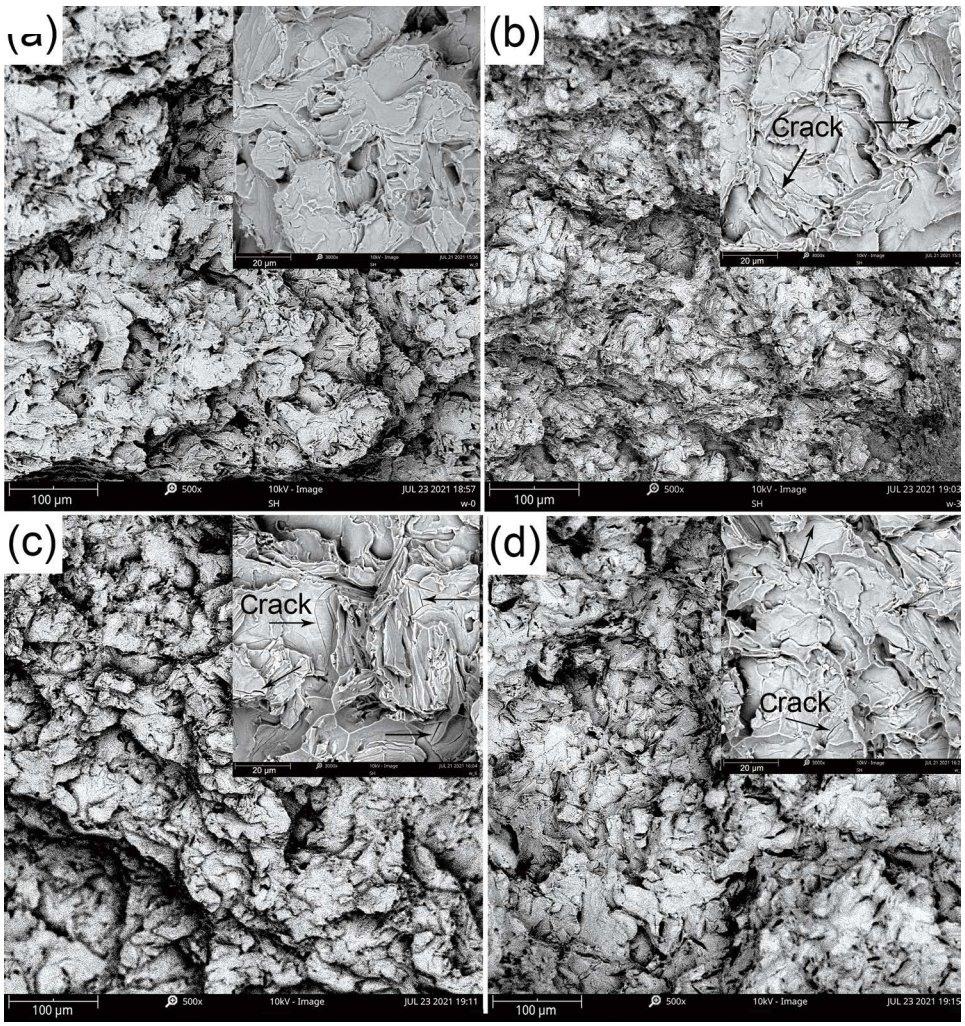

Fig. 11: Mechanical properties of Al-12Si alloys modified with different amounts of Al-12Si/ZnS powder: (a) non-modified alloy; (b) 12.5 wt.%; (c) 17.5 wt.%; (d) 22.5 wt.%

also occurs at the grain boundaries. The different tensile fracture behaviors were caused by two distinct eutectic Si morphologies in the alloy: long needle-like and short rod shape. With the addition of Al-12Si/ZnS powder, the long needle-like eutectic Si is refined into short-rod and globular shape. Due to the spheroidization of eutectic Si, which can reduce stress concentrations at grain boundaries, crystalline fracture decreases, and the number of cleavage plane increases, as shown in Fig. 11(b), (c) and (d). Therefore, crack propagation is more likely to be initiated inside the crystal owing to improved strength at the grain boundary, as evidenced by the cracks shown in the insets of Figs. 11(b), (c), and (d). Thus, fracture of Al-12Si alloys modified by Al-12Si/ZnS powder is dominated by transgranular fracture supplemented by intergranular fracture.

3.4 Refinement mechanism of Al-12Si/ZnS powder

Below 1,020 °C, the crystal structure of ZnS is cubic crystal, which is consistent with the XRD analysis. Table 2 shows the mismatch between the Si and ZnS phase based on the edge-to-edge matching (E2EM) model. The main possible matching planes of ZnS with Si are {111}, {220}, and {311}, which have in-plane misfit (F_p) values of 0.399%, 0.422%, and 0.275%, respectively. The interatomic spacing misfit (F_r) values between $<1\bar{2}1>_{Si\&ZnS}$, $<1\bar{1}0>_{Si\&ZnS}$, and $<1\bar{2}\bar{1}>_{Si\&ZnS}$ were calculated as 0.456%, 0.458%, and 0.456%, respectively. Both F_p and F_r are far lower than 6%, which illustrates perfect lattice matching between ZnS and Si. The above analysis demonstrates that ZnS phases can effectively act as heterogeneous nucleation sites of Si.

To further characterize the crystal orientation of ZnS, HRTEM was performed. The results are shown in Fig. 12. As seen in Fig. 4 and Fig. 7, the main planes of ZnS and Si are (111), (311), and (220). Figure 12 shows the main planes of Si are clearly (111). The images further reveal that the orientations of all planes are practically unanimous. The (111) plane of ZnS is parallel to the (111) plane of Si, and the ZnS phase grows in the same direction as the Si phase. Transition zones of several nanometers in thickness clearly exist between the ZnS and Si phase. The crystallinity of ZnS is previously increased with trisodium citrate but is not perfect [34], which is consistent with the XRD analysis above. However, the structural mismatch between the overlayer (ZnS) and substrate (Si) due to the transition zone results in the switch from the Frank-van der Merwe (FM) growth mode (2D morphology) to the Volmer-Weber (VW) growth mode (3D morphology) [35]. In other words, the transition zones are the key to the growth of ZnS particles on the surface of Al-12Si powder. In general, the crystal orientation of Si and ZnS is almost the same, which also indicates that ZnS can act as a heterogeneous nucleation site of Si. Unfortunately, the coherence relationship between Si and ZnS was not directly observed in Al-12Si alloy under HRTEM. To indirectly illustrate the coherent relationship between Si and

Table 2: Edge-to-edge mismatching between Si and ZnS

Matching planes	F_p (%)	Matching rows	F_r (%)
Si{111}//ZnS{111}	0.399	$Si<1\bar{2}1>$//$ZnS<1\bar{2}1>$	0.456
Si{220}// ZnS {220}	0.422	$Si<1\bar{1}0>$// $ZnS<1\bar{1}0>$	0.458
Si {311}// ZnS {311}	0.275	$Si<1\bar{2}\bar{1}>$// $ZnS<1\bar{2}\bar{1}>$	0.456

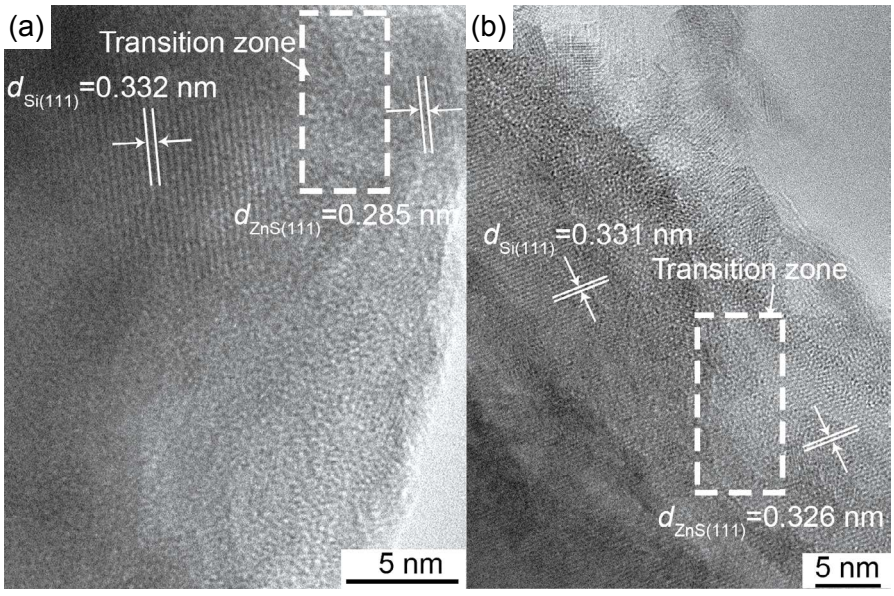

Fig. 12: HRTEM images of as-prepared Al-12Si/ZnS powder

ZnS in X-ray diffraction analysis, monocrystalline Si slice/ZnS and polycrystalline Si slice/ZnS were used as the analytical reference.

The mechanism of refinement of Al-12Si/ZnS powder is illustrated in Fig. 13. Nano-sized ZnS particles on the surface of the Al-24Si/ZnS promote wetting by the melt, which also increases the number of crystal nuclei. In contrast, nano-sized ZnS particles dispersed on the surface are easily dispersed into the melt owing to the presence of non-agglomerated particles. As the powder melts, the ZnS particles are released into the melt, thereby reducing the undercooling of the silicon phase and acting as Si nucleation sites. The Si atoms nucleate preferentially with a ZnS core and grow into short rod-like or globular Si phase. At the same time, α-Al nucleates and grows until it comes into contact with the Si phase. The size of the α-Al phase decreases with further refinement of the Si phase. In summary, sufficient quantities of ZnS provide excellent heterogeneous nuclei of Si due to the low mismatch degree, good dispersion, and wettability.

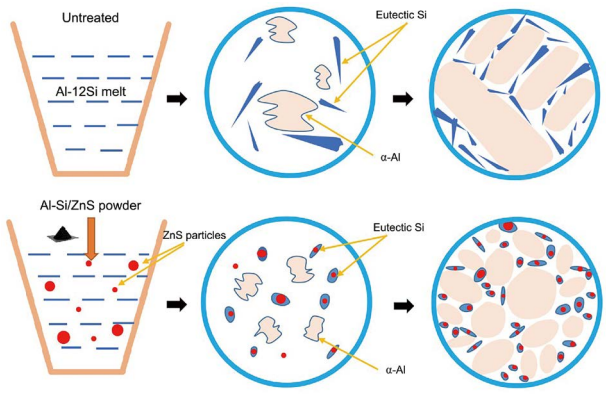

Fig. 13: Refinement mechanism of Al-12Si/ZnS powder

4 Conclusions

(1) Al-12Si/ZnS powder was successfully prepared via a simple chemical bath deposition method. Wettability was enhanced by the incomplete crystallization of nano-ZnS particles distributed on the surface of Al-12Si alloy powder.

(2) The inoculant Al-12Si/ZnS can refine the eutectic Si phase in Al-12Si cast alloys. The morphology of eutectic Si changes from needle-like to short rod-like or even spherical in shape with the increase of Al-12Si/ZnS powder. The refinement mechanism is nucleation of Si from ZnS nucleation cores, accommodated by the low in-plane misfit (F_p) values and interatomic spacing misfit (F_r) values of ZnS with Si.

(3) The best refinement effect for needle-like eutectic Si can be achieved in the Al-12Si cast alloy with 17.5% Al-12Si/ZnS powder. Eutectic Si is modified into a coral-like spherical shape with the average size of about 6.53 μm.

(4) The hardness, tensile strength and elongation of Al-12Si alloy modified with 17.5% Al-12Si/ZnS powder increased by 6.3%, 16.19% and 55.35%, respectively, compared to the unmodified Al-12Si alloy. Its fracture behavior is dominated by transgranular fracture supplemented by intergranular fracture.

Acknowledgements

The authors gratefully acknowledge financial support from the National Natural Science Foundation of China (Grant No. 51672145).

References

[1] Zhang Haitao, Zuo Kesheng, Han Xing, et al. Effects of P+Cr complex modification and solidification conditions on microstructure of hypereutectic Al-Si alloys by wedge-shaped copper mould casting. China Foundry, 2014, 11(6): 481–486.
[2] Fan Zhen, Song Wei, Zhang Huarui, et al. Effect of holding pressure on density and cooling rate of cast Al-Si alloy during additive pressure casting. China Foundry, 2019, 16(6): 363–370.
[3] Bo Dang, Zeng-yun Jian, Jun-feng Xu, et al. Effect of phosphorus and heat treatment on microstructure of Al-25%Si alloy. China Foundry, 2017, 14(1): 10–15.
[4] Matsuura K, Kudoh M, Kinoshita H, et al. Precipitation of Si particles in a super-rapidly solidified Al-Si hypereutectic alloy. Mater. Chem. Phys, 2003, 81(2): 393–395.
[5] Hatk, Park W J, Ahn S H, et al. Fabrication of spray-formed hypereutectic Al-25Si alloy and its deformation behavior. Journal of Materials Processing Technology, 2002, 130-131: 691-695.
[6] Jian X G, Han Q Y. Formation of hypereutectic silicon particles in hypoeutectic Al-Si alloys under the influence of high-intensity ultrasonic vibration. China Foundry, 2013, 10(2): 118–123.
[7] Liao H C, Sun G X. Development on mechanisms of the eutectic Si modification. Foundry, 2003, 52(12): 1127–1129.
[8] Vijayan V, Prabhu P. Review of microstructure evolution in hypereutectic Al–Si alloys and its effect on wear properties. Transactions of the Indian Institute of Metals, 2014, 67(1): 1–18.
[9] Lu Shuzu, Hellawell A. Modification of Al-Si alloys: microstructure, thermal analysis, and mechanisms. JOM, 1995, 47(2): 38–40.
[10] Roehling J D, Coughlin D R, Gibbs J W, et al. Rapid solidification growth mode transitions in Al-Si alloys by dynamic transmission electron microscopy. Acta Materialia, 2017, 131: 22–30.
[11] Liu W Y, Xiao W L, Xu C, et al. Synergistic effects of Gd and Zr on grain refinement and eutectic Si modification of Al-Si cast alloy. Materials Science and Engineering: A, 2017, 693(5): 93–100.
[12] Zhang Y B, Kateryna S, Li T J. Effect of ultrasonic treatment on formation of iron-containing intermetallic compounds in Al-Si alloys. China Foundry, 2016, 13(5): 316–321.
[13] Knuutinen A, Nogita K, McDonald S D, et al. Modification of Al-Si alloys with Ba, Ca, Y and Yb. Journal of Light Metals, 2001, 1(4): 229–240.
[14] Subroto T, Miroux A, Bouffier L, et al. Formation of hot tear under controlled solidification conditions. Metallurgical & Materials Transactions A, 2014, 45(6): 2855–2862.
[15] Nogita K, Yasuda H, Yoshiya M, et al. The role of trace element segregation in the eutectic modification of hypoeutectic Al-Si alloys. Journal of Alloys & Compounds,2010, 489(2): 415–420.
[16] Tsai Yuchou, Lee Sheng-long, Lin Chih-kuang. Effect of trace Ce addition on the microstructures and mechanical properties of A356 (Al-7Si-0.35Mg) aluminum alloys. Journal of the Chinese Institute of Engineers, 2011, 34(5): 609–616.
[17] Choi Hongseok, Konishi Hiromi, Li Xiaochun. Al_2O_3 nanoparticles induced simultaneous refinement and modification of primary and eutectic Si particles in hypereutectic Al-20Si alloy.

Materials Science and Engineering: A, 2012, 541(1): 159–165.
[18] Zhang Henghua, Duan Haili, Shao Guangjie, et al. Microstructure and mechanical properties of hypereutectic Al-Si alloy modified with Cu-P. Rare Metals, 2008, 27(1): 59–63.
[19] Wang W, Guo F X, Gai Z G, et al. The formation of nanoparticles and their competitive interaction with twins during eutectic Si growth. Materials, 2018, 11(8): 1040.
[20] Lu Liming, Nogita K, Dahle A K. Combining Sr and Na additions in hypoeutectic Al–Si foundry alloys. Materials Science and Engineering: A, 2005, 399(1/2): 244–253.
[21] Cardinale A M, Maccio D, Luciano G, et al. Thermal and corrosion behavior of as cast Al-Si alloys with rare earth elements. Journal of Alloys & Compounds, 2017, 695: 2180–2189.
[22] Ahmad R, Asmael M B A. Influence of lanthanum on solidification, microstructure, and mechanical properties of eutectic Al-Si piston alloy. Journal of Materials Engineering and Performance, 2016, 25(7): 2799–2813.
[23] Ren B, Liu Z X, Zhao R F, et al. Effect of Sb on microstructure and mechanical properties of Mg_2Si/Al-Si composites. Transactions of Nonferrous Metals Society of China, 2010, 20(8): 1367–1373.
[24] Nogita K, Mcdonald S D. Eutectic modification of Al-Si alloys with rare earth metals. Materials Transactions, 2004, 45(2): 323–326.
[25] Liu L, Samuel A M, Samuel F H, et al. Characteristics of α-dendritic and eutectic structures in Sr-treated Al-Si casting alloys. Journal of Materials Science, 2004, 39(1): 215–224.
[26] Kawther A H, Ian S, Fan Z Y. Refinement of primary silicon crystals by novel Al-ZnS master alloy in solidification of hypereutectic Al-Si Alloys. In: Edward Williams (Eds), Light Metal 2016. Switzerland: Springer International Publisher, 2016: 271–273.
[27] Li C D, Si W Q, Zhao M, et al. A new Al-ZnS master alloy designed for modifying hypereutectic Al-Si alloy and its refinement performance on primary Si. Advanced Materials Research, 2015, 1088: 242–244.
[28] Li C D, Sun C H, Si W Q, et al. Effects of ZnS modification on primary Si in hypereutectic Al-Si alloy. China Foundry, 2017, 14(2): 93–97.
[29] Zhang J H, Xing S M. Modifying elements and their interaction in Al-Si alloy. Materials Review, 2018, 32(6): 1870–1877.
[30] Quested T E, Greer A L. The effect of the size distribution of inoculant particles on as-cast grain size in aluminium alloys. Acta Materialia, 2004, 52(13): 3859–3868.
[31] Zhang Y, Dang X Y, Jin J, et al. ZnS thin film deposited with chemical bath deposition process directed by different stirring speeds. Applied Surface Science, 2010, 256(22): 6871–6875.
[32] Goudarzi A, Aval G M, Sahraei R, et al. Ammonia-free chemical bath deposition of nanocrystalline ZnS thin film buffer layer for solar cells. Thin Solid Films, 2008, 516(15): 4953–4957.
[33] Liao Harris, Chang Yeonghwa, Chen Yangfang, et al. Fabrication of ZnSe quantum dots under Volmer–Weber mode by metalorganic chemical vapor deposition. Applied Physics Letters, 1997, 70(17): 2256–2258.
[34] Poulomi Roy, Jyoti R. Ota, Suneel Kumar Srivastava. Crystalline ZnS thin films by chemical bath deposition method and its characterization. Journal of Functional Materials, 2006, 515: 1512–1515.
[35] H. Brune. Encyclopedia of Materials: Science and Technology. Elsevier Science Ltd., 2001.